ENHANCED LESION VISUALIZATION IN IMAGE-GUIDED NONINVASIVE SURGERY WITH ULTRASOUND PHASED ARRAYS

Hui Yao, Pornchai Phukpattaranont and Emad S. Ebbini

Department of Electrical and Computer Engineering
University of Minnesota
Minneapolis, MN 55455

Abstract- **We describe dual-mode ultrasound phased arrays for noninvasive image-guided surgical applications. In particular, we address the problem of real-time visualization of thermal lesion formation in the target (e.g., tumor) tissue using the therapeutic arrays. Post beamfroming filter bank image reconstruction with nonlinear compounding is utilized to improve the lesion contrast in the (typically) very low-contrast ultrasound images. It is shown that the new image reconstruction algorithm leads to measurable improvement in lesion contrast on the order of 6 - 15 dB. This leads to significant improvement in lesion detectability and size estimation by standard segmentation techniques for speckle imagery. Experimental results strongly suggest that 2^{nd} Harmonic imaging could play an important role in the enhancement of real-time lesion visualization.**

1. INTRODUCTION

Image guidance has long been recognized as the "enabling technology" for noninvasive thermal surgery. Highly refined energy application devices have been developed and for years. However, without reliable imaging techniques for visualization of thermal lesions, noninvasive thermal surgery has failed to find widespread acceptance in the clinic. Recently, image guidance methods based on well established imaging modalities like MRI[3], CT[5], or ultrasound [4, 8] have been proposed. Other imaging modalities are also being developed and may become available in the foreseeable future[6, 7].

An area unique to ultrasound that could revolutionize the field of image guided surgery is the development of a new generation of dual-mode high-power phased array systems capable of both imaging and therapy [8, 9]. These piezocomposite transducers can produce focal intensity levels needed for ablative and coagulative thermal surgery with high precision. Furthermore, the operating bandwidth of such transducers allows for imaging the treatment region with adequate image quality to delineate important landmarks within and around the target volume. With these capabilities, it is possible to operate these arrays in a "self-registration" mode whereby the imaging capabilities of the array are utilized in characterization of the tissue response precisely at the expected lesion location. This is due to the fact that the beamforming is common to both the imaging and therapy modes. The main challenge to this approach is the low-contrast nature of speckle-ridden ultrasound images. This paper addresses a new post beamforming filter bank image reconstruction algorithm with nonlinear spatially weighted compounding algorithm to mitigate this problem. The design of this algorithm is motivated by the nonlinear nature of ultrasound propagation in tissue and the fact that thermal lesions are known to have increased level of harmonic generation. Experimental results demonstrate the potential of the new algorithm in both enhancing the lesion contrast and size/shape analysis.

Funded by Grant DAMD 17-01-1-330 from the US Army Medical Research and Materiel Command.

2. IMAGE FORMATION MODEL

Figure 1 summarizes the image acquisition and image formation model. A 64-element array optimized for maximum energy delivery at 1 MHz operating frequency is used for lesion formation in sample tissue. Lesions are formed by focusing the array at a point within the target and maintaining high-power output for time intervals on the order of seconds (1 - 5 seconds typical). The power is interrupted for short intervals (milliseconds) to acquire image data by transmitting short (μs) pulses from all 64-elements and receiving on selected elements using a matrix switch. Once the image data set is collected, RF beamforming is performed to form standard echographic images of the target region. It is well known that these images have very low contrast due to the coherent nature of image acquisition which produces speckle. This renders the lesion detection very difficult using ultrasound.

Report Documentation Page

Report Date	Report Type	Dates Covered (from... to)
25 Oct 2001	N/A	-

Title and Subtitle Enhanced Lesion Visualization in Image-Guided Noninvasive Surgery With Ultrasound Phased Arrays	**Contract Number**
	Grant Number
	Program Element Number
Author(s)	**Project Number**
	Task Number
	Work Unit Number
Performing Organization Name(s) and Address(es) Department of Electrical and Computer Engineering University of Minnesota Minneapolis, MN 55455	**Performing Organization Report Number**
Sponsoring/Monitoring Agency Name(s) and Address(es) US Army Research, Development & Standardization Group (UK) PSC 802 Box 15 FPO AE 09499-1500	**Sponsor/Monitor's Acronym(s)**
	Sponsor/Monitor's Report Number(s)

Distribution/Availability Statement
Approved for public release, distribution unlimited

Supplementary Notes
Papers from 23rd Annual International Conference of the IEEE Engineering in Medicine and Biology Society, October 25-28, 2001, held in Istanbul, Turkey. See also ADM001351 for entire conference on cd-rom.

Abstract

Subject Terms

Report Classification unclassified	**Classification of this page** unclassified
Classification of Abstract unclassified	**Limitation of Abstract** UU

Number of Pages
4

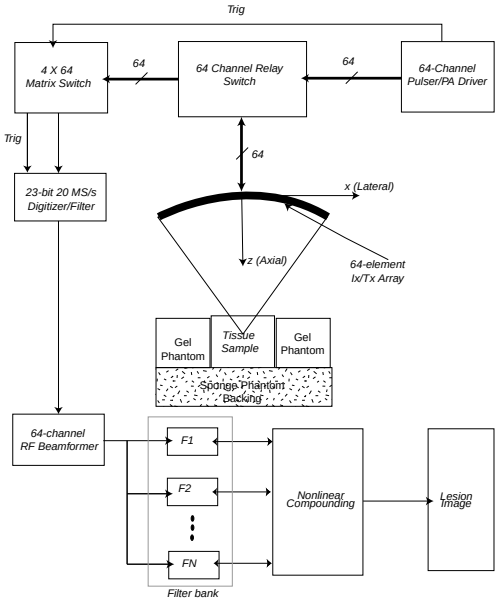

Fig. 1. Image Acquisition and Image Reconstruction Algorithm

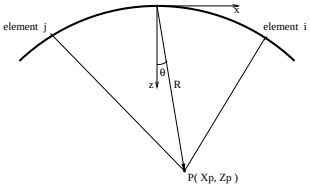

Fig. 2. Coordinate system used in the synthetic aperture imaging system.

2.1. Synthetic aperture imaging

Images were obtained using a full synthetic aperture technique [10]. The image pixel at coordinates (x_p, z_p) was therefore computed by (Fig. 2):

$$I(x_p, z_p) = \sum_{i=1}^{64} \sum_{j=1}^{64} A_i \cdot B_j \cdot s_{i,j} \left[\left(R_{ip} + R_{jp} \right) / c \right], \quad (1)$$

where i is the transmit element index, j is the receive element index, A_i is the transmit apodization weight at element i, B_j is the receive apodization weight at element j, R_{ip} and R_{jp} are the distances from the transmit and receive elements, respectively, from the image pixel, c is the speed of sound in the medium being imaged, and $s_{i,j}(t)$ is the echo acquired when transmitting with element i and receiving with element j. Specialized image reconstruction programs were written to evaluate the intensity at (x_p, z_p) in either $(r, \sin\theta)$ or Cartesian coordinates.

2.2. Single-Transmit Imaging

The synthetic aperture imaging algorithm described above can be used to produce the highest quality conventional images that can be expected from a given array. However, due to the fact that transmit beams are synthesized by superposition of single-element transmit patterns, the nonlinear interactions of the real-time transmit beams cannot be accounted for using this imaging algorithm. Therefore, we have modified our 64-channel phased array driver to allow for pulsed transmission on all 64 channels simultaneously. This allowed us to use the full power of the transmit beams and, therefore, observe their nonlinear interactions with the tissue media. The image formation process due to a single-transmit focused beam is a modified version of Eq. (1) as follows:

$$I(x_p, z_p) = \sum_{j=1}^{64} B_j \cdot s_j \left[\left(R_0 + R_{jp} \right) / c \right], \quad (2)$$

where $s_j(t)$ is the received waveform at element j due to the transmitted beam and R_0 is a fixed distance determined by the focal depth of the transmit beam. All other quantities in Eq. (2) are the same as their counterparts in Eq. (1). It should be noted that beamforming is performed in the RF domain using true delays, i.e., no baseband conversion is done. This retains all the frequency components in the beamformed data for postbeamforming filtering operations described below.

2.3. Post Beamforming Filtering

Since beamforming is performed in the RF domain, all the frequency components in the received echo signals are retained. This is important since the echo signals can be expected to contain a mix of harmonics (and possibly subharmonics) depending on the nonlinearity of the tissue medium being imaged. This is especially true for the single-transmit imaging mode where the transmit power is sufficiently high to produce harmonic components in nonlinear tissue media. Postbeamforming filtering can be used to isolate specific harmonic components and/or enhance axial resolution if the SNR of the system is sufficiently high. Algorithms for postbeamforming filterbank image reconstruction for pulse-echo ultrasound can be found in [11]. For the purposes of this paper, the filter bank is formed of bandpass filters with center frequencies at a set of preselected harmonics (or subharmonics).

2.4. Nonlinear Compounding

Ultrasound propagation in tissue media is inherently nonlinear. RF echo signals obtained using modern scanners with wideband transducers carry harmonic components that are

generated by the medium nonlinearity, i.e., they are not part of the originally transmitted imaging pulses. Since the tissue nonlinearity parameter exhibits higher contrast between various tissue compared to tissue reflectivity, imaging this parameter can lead to higher contrast images of soft tissue. For a variety of physical reasons, it is well known that thermal lesions generate higher harmonics at levels higher than normal tissues. By careful design of the transmit/receive beamforming and the post beamforming reconstructions filters, high contrast images of lesions can be formed from ultrasound images formed at the fundamental and some of its higher harmonics. In general, an optimal compounding rule must be derived based on statistical model of the imaged region and the expected lesion size/location. Furthermore, the quality of the beamforming at different harmonics or scales will be spatially heterogeneous. For example, since the array sampling function (in wavelengths) is coarser at the higher harmonics, images formed at these frequency will have high contrast along the axis of the transmit beam, but the contrast deteriorates away from the main axis. Furthermore, since the harmonics are orders of magnitudes smaller than the fundamental, compounding is performed with log-compressed images after appropriate scaling. Therefore, with reference to Figure 1, the compounding is performed in two stages:

1. The outputs of the filterbank are envelope detected, scaled, and log compressed.

2. A spatially-weighted sum of the harmonic components is performed. The weighting function is derived from the spatial contrast function (SCF) of the imaging array at the different harmonics.

Assuming that the envelope-detected, normalized and log-compressed images obtained from the filterbank are given by $I_1, I_2, \ldots, I_N$, then the compounded image is given by:

$$I(x,y) = \sum_{i=1}^{N} W_i S_i(x,y) I_i(x,y) \qquad (3)$$

where W_i is a weighting function reflecting the relative energy at the harmonic with respect to the fundamental at the (expected) lesion location and $S_i(x,y)$ is the SCF associated with the ith harmonic. The SCFs at the different harmonic components are computed from the inverse of the beam patterns when the transmit beam is focused at the center of the (expected) lesion.

3. RESULTS

Images shown in Figure 3 and Figure 4 demonstrate the basic ideas behind the proposed image compounding algorithm. The figures show images obtained before and after lesion formation in an *ex-vivo* liver tissue samples. The expected lesions are cigar-shaped with length of 10 mm and width of 2 - 3 mm. All images are shown at 25 dB dynamic range and have the same axial and lateral extent. In both experiments, the lesion was formed at the geometric center of the array and was expected between 90 and 100 mm in the axial direction. All images show the front surface of the sample at 80 mm and the sponge backing phantom at 120 mm. For each experiment, two pairs of images are shown, one before and one after the lesion formation. Images shown on the left hand side of each figure show the target before lesion formation while images on the right hand side show the target after lesion formation. The images on top of each figure are formed at the fundamental (1 MHz 50% bandwidth) while those at the bottom of each figure are formed at the 2nd harmonic (2MHz 40% bandwidth). Each pair of images is displayed on a log scale and normalized such that the 0 dB corresponds to the maximum of the image on the RHS, i.e., the image of the target after lesion formation. The first experiment represent a fairly homo-

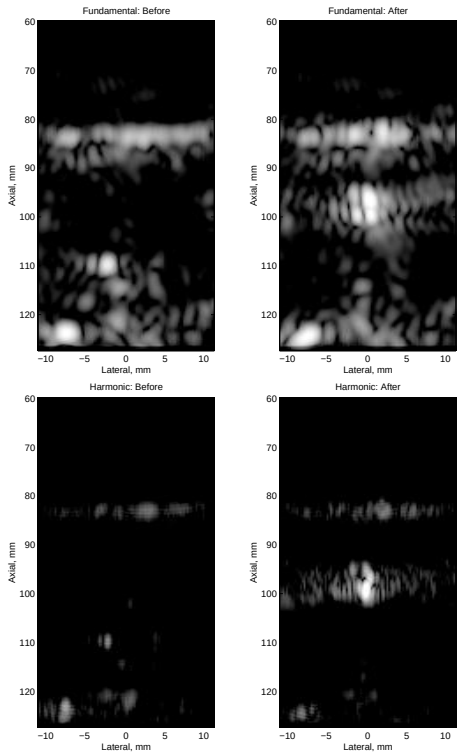

Fig. 3. Images before and after formation of Lesion 1.

geneous target tissue while the second has a pair of blood vessels at the target location as can be seen from the images taken before lesion formation. While both the fundamental and harmonic images show enhanced lesion contrast in both cases, the harmonic images show a net increase in contrast by 22 dB in the second case. On the other hand, the

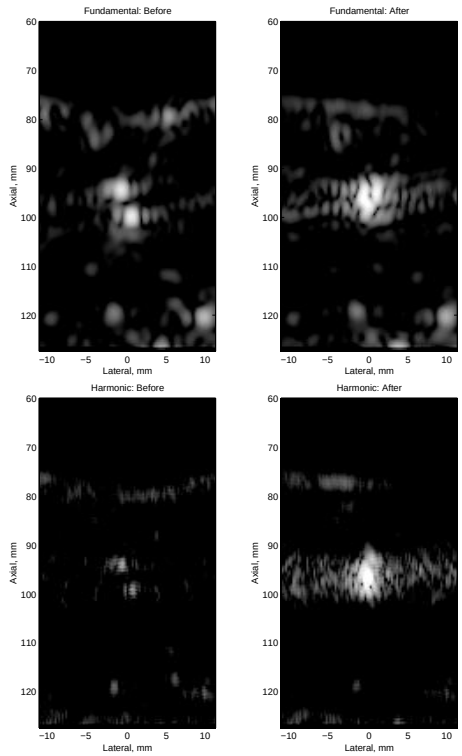

Fig. 4. Images before and after lesion 2.

net increase in contrast at the fundamental is about 7 dB. In addition, the spatial definition of the lesion in the harmonic images is superior to the fundamental. The two cases shown also illustrate the need for nonlinear compounding with a spatial weighting function as implied by (3). While the harmonic images are superior both in terms of definition and contrast near the main axis of the transmit beam, the fundamental images better represent the tissue state off-axis.

4. CONCLUSIONS

We have shown that post beamforming filterbank reconstruction of ultrasound images at selected frequencies sensitive to harmonic generation in nonlinear media produces images appropriate for compounding. The main features (thermal lesions) are sufficiently correlated while the speckle noise is largely uncorrelated. The enhanced nonlinear tissue response at the lesion location is most probably due to formation of microbubbles that resonate nonlinearly producing 2^{nd} and higher harmonic frequencies in the echo data. Experimental work for validation of this hypothesis is currently underway.

5. REFERENCES

[1] B. Fallone, P. Moran, and E. Podgorsak, "Noninvasive thermometry with a clinical X-ray scanner," *Med. Phys.*, vol. 9, no. 5, pp. 715–721, 1982.

[2] D. Parker, "Applications of NMR imaging in hyperthermia: An evaluation of the potential for localized tissue heating and noninvasive temperature monitoring," *IEEE Trans. Biomed. Eng.*, vol. 31, no. 1, pp. 161–167, 1984.

[3] J. Poorter, C. Wagter, Y. Deene, C. Thomsen, F. Stahlberg, and E. Achten, "Noninvasive MRI thermometry with the proton resonance frequency (PRF) method: In vivo results in human muscle," *Magn. Reson. Med.*, vol. 33, pp. 74–81, 1995.

[4] N. Sanghvi *et al.*, "Noninvasive surgery of prostate tissue by high-intensity focused ultrasound," *IEEE Trans. UFFC*, vol. 43, no. 6, pp. 1099–1110, Nov. 1996.

[5] J. Jenne, M. Bahner, J. Spoo, P. Huber, R. Rastert, I. Simiantonakis, W. Lorenz, and J. Debus, "CT on-line monitoring of HIFU therapy," *IEEE Ultrason. Symp.*, 1997.

[6] K.Paulsen, M.Moskowitz, T.Ryan, S.Mitchell, and P.Hoopes, "Initial *in vivo* experience with EIT as a thermal estimator during hyperthermia," *Int. J. Hyperthermia*, vol. 12, no. 5, pp. 573–591, Sept. 1996.

[7] P.Meaney, K.Paulsen, A.Hartov, and R.Crane, "Microwave imaging for tissue assessment: Initial evaluation in multitarget tissue-equivalent phantoms," *IEEE Trans. Biomed Eng.*, vol. 43, no. 9, pp. 878–890, Sept. 1996.

[8] E. Ebbini, P. VanBaren, and C. Simon, "Image-guided noninvasive surgery with ultrasound phased arrays," *SPIE Bios: Surgical Applications of Energy*, 1998.

[9] C. Simon, J. Shen, T. Hall, and E. Ebbini, "Combined ultrasound image guidance and therapy using a therapeutic phased array," *SPIE: Medical Imaging 1998*, vol. 3341, pp. San Diego, Feb. 1998.

[10] K. Thomenius, "Evolution of ultrasound beamformers," *IEEE Ultrason. Symp.*, pp. 1615–1622, Nov. 1996.

[11] J. Shen and E. S. Ebbini. "Filter-based coded-excitation system for high speed ultrasonic". *IEEE Trans. Medical Imaging*, 45(6), December 1998.